Lidar configurations for wind turbine control

Mirzaei, Mahmood; Mann, Jakob

Published in:
Journal of Physics: Conference Series (Online)

Link to article, DOI:
10.1088/1742-6596/753/3/032019

Publication date:
2016

Document Version
Publisher's PDF, also known as Version of record

Lidar configurations for wind turbine control

Mahmood Mirzaei and Jakob Mann

DTU Wind Energy, Technical University of Denmark, Frederiksborgvej 399, 4000 Roskilde, Denmark

E-mail: mmir@dtu.dk, jmsq@dtu.dk

Abstract. Lidar sensors have proved to be very beneficial in the wind energy industry. They can be used for yaw correction, feed-forward pitch control and load verification. However, the current lidars are expensive. One way to reduce the price is to use lidars with few measurement points. Finding the best configuration of an inexpensive lidar in terms of number of measurement points, the measurement distance and the opening angle is the subject of this study. In order to solve the problem, a lidar model is developed and used to measure wind speed in a turbulence box. The effective wind speed measured by the lidar is compared against the effective wind speed on a wind turbine rotor both theoretically and through simulations. The study provides some results to choose the best configuration of the lidar with few measurement points.

1. Introduction

Lidar sensors have proved to be very beneficial in the wind energy industry for different applications such as yaw corrections [5], pitch control [13, 6, 9] and power and loads verifications [4]. There are different issues with lidar measurements. Lidars measure the line of sight (LOS) wind speed. This means that measuring off-center of the rotor disc, assuming lidar is mounted on the nacelle, provides measurements that are taking into account wind speed components parallel to the rotor disc. This is especially problematic in lidars with few measurement points and when the opening angle of the lidar is increased. In this case the effect of the transverse wind speed components (v and w components where u component is perpendicular to the rotor disc) becomes significant. Lidars also measure along a line instead of a focus point and this leads to a weighted average of the wind speed over the measurement line (see also eq. 2). As the measurement distance increases the focus area expands and the effect of wind speeds off the focus point increases. Besides, measuring very close to the rotor disc means that the effect of the induction zone is prominent in the measurements. Taking the factors mentioned above into account makes coming up with the best lidar configuration not a trivial task. In this paper an analysis on the best configuration of a lidar with a few number of measurement points is given. The analysis includes the optimum number of measurement points as well as the location of them, taking into account the trade-off between increased accuracy of the effective wind speed measurement and increased cost of adding more measurement points. The basic configuration of the lidar in the case of four beams is shown in figure 1. The lidar is not focussed at a point but rather in a pencil thin many meters long volume [11, 1].

The paper presents two analysis methods. In the first method, explained in section 2 a theoretical analysis is given based on the Mann spectral tensor [7]. A similar approach based on statistics was used in [12], but it was based on auto-spectra and exponential coherences [3],

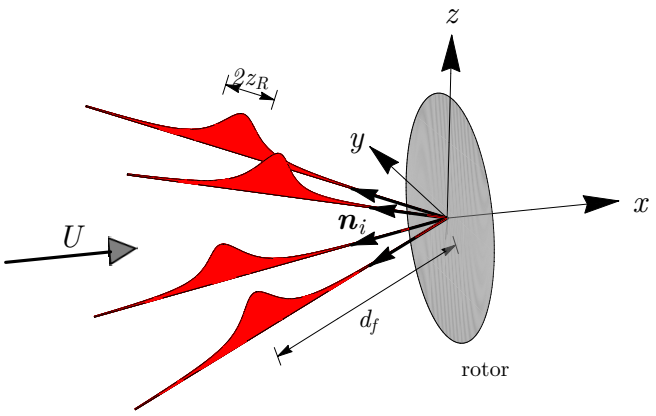

Figure 1. Geometry of the rotor and lidars. The x-axis is in the mean wind direction. $N = 4$ lidar beams point upwind in the directions determined by the unit vectors $\boldsymbol{n}_i$. The beams are focussed at a distance d_f from the instrument at the center of the rotor, and their weighting functions has full width at half maximum z_R, see (3).

not a spectral tensor.

The second method, explained in section 3, is based on analysis of the time series obtained through simulations. In this method several turbulence boxes also using the Mann model are produced. A lidar model is developed in which the different physics and limitations of the instrument is implemented. Then the lidar is used to measure the effective wind speed in the turbulence box. The rotor effective wind speed is also measured and compared against the lidar measurements.

2. Theoretical analysis

The lidar is assumed to be mounted close to the center of the rotor with N beams pointing in various directions.

The wind field is described by a vector field $\boldsymbol{u}(\boldsymbol{x})$ where the time argument is eliminated because Taylor's frozen turbulence hypothesis is assumed [10]. The mean value of the homogeneous velocity field is $\langle \boldsymbol{u}(\boldsymbol{x}) \rangle = (U, 0, 0)$, so the coordinate x_1 is in the mean wind direction. In other words the wind field as a function of space and time can be written as

$$\boldsymbol{u}(\boldsymbol{x}, t) = \boldsymbol{u}(x_1 - Ut, x_2, x_3) \tag{1}$$

The origo of the coordinate system is at the center of the rotor (at time zero), which coincides with the position of the lidar.

The lidar beams are focussed at some distance d_f from the instrument and the i'th beam is pointing the the direction defined by the unit vector $\boldsymbol{n}_i$. The first coordinate n_{i1} of $\boldsymbol{n}_i$ will always be negative because the beam are pointing upwind of the rotor. The lidar is not focussed at a point but rather in a pencil thin many meters long volume [11, 1]. The velocity measured by the i'th lidar beam may be approximated by

$$v_i(\boldsymbol{x}) = \int_{-\infty}^{\infty} \boldsymbol{n}_i \cdot \boldsymbol{u}(s\boldsymbol{n}_i + \boldsymbol{x}) \phi(s - d_f) ds, \tag{2}$$

where the weighting function for a continuous-wave lidar typically is approximated by

$$\phi(s) = \frac{1}{\pi} \frac{z_R}{z_R^2 + s^2} \tag{3}$$

with z_R being the Rayleigh length [14]. The argument $\boldsymbol{x}$ in (2) is the position of the lidar with a first component decreasing with time as $-Ut$ using Taylor's hypothesis.

The instantaneous longitudinal wind speed derived from the lidar is a linear combination of the N line-of-sight velocities (2). If $\boldsymbol{m}$ is a vector of length N with the weights of the linear combination, then the lidar estimated longitudinal wind speed is

$$u_L = \boldsymbol{m} \cdot \boldsymbol{v} \tag{4}$$

The purpose of the analysis is to find the combination of unit vectors $\boldsymbol{n}_i$ $(i = 1, ..., N)$ and focus distances d_f, which typically do not differ from beam to beam, that minimizes the difference between u_L and the rotor averaged longitudinal wind speed

$$u_R(\boldsymbol{x}) = \frac{1}{\pi R^2} \iint\limits_{\text{rotor}} u_1 \left(\boldsymbol{x} + (0, x_2', x_3')\right) dx_2' dx_3', \tag{5}$$

where R is the radius of the rotor. One could also choose not to weight the wind speed evenly over the rotor, but to put less emphasis on hub and the tip regions.

If Δx is the positive distance between the vertical plane with the lidar beam foci and the rotor plane (which for simplicity is also assumed to be vertical), then we want to minimize error variance

$$\sigma_e^2 = \left\langle \left(u_L(\boldsymbol{x} + (\Delta x, 0, 0)) - u_R(\boldsymbol{x})\right)^2 \right\rangle, \tag{6}$$

or equivalently

$$\sigma_e^2 = \left\langle \left(u_L(\boldsymbol{x}) - u_R(\boldsymbol{x} - (\Delta x, 0, 0))\right)^2 \right\rangle. \tag{7}$$

The separation Δx is equivalent to delaying the measurements from the lidar a time period $t = \Delta x / U$.

2.1. Mean squared error expressed by a spectral tensor

The wind field can be written as a Fourier integral

$$\boldsymbol{u}(\boldsymbol{x}) = \int \boldsymbol{u}(\boldsymbol{k}) \mathrm{e}^{\mathrm{i}\boldsymbol{k}\cdot\boldsymbol{x}} d\boldsymbol{k} \Leftrightarrow \boldsymbol{u}(\boldsymbol{k}) = \frac{1}{(2\pi)^3} \int \boldsymbol{u}(\boldsymbol{x}) \mathrm{e}^{-\mathrm{i}\boldsymbol{k}\cdot\boldsymbol{x}} d\boldsymbol{x} \tag{8}$$

where we are a bit slack and do not use the more rigorous Fourier-Stieltjes notation [2, 8]. The ensemble average of the absolute squared Fourier coefficients is the spectral tensor

$$\left\langle u_i^*(\boldsymbol{k}) u_j(\boldsymbol{k'}) \right\rangle = \Phi_{ij}(\boldsymbol{k}) \delta(\boldsymbol{k} - \boldsymbol{k'}) \tag{9}$$

and it is according to the Wiener-Khinchin theorem related to the covariance tensor $R_{ij}(\boldsymbol{r}) \equiv \langle u_i(\boldsymbol{x}) u_j(\boldsymbol{x} + \boldsymbol{r}) \rangle$ by

$$\Phi_{ij}(\boldsymbol{k}) = \frac{1}{(2\pi)^3} \int R_{ij}(\boldsymbol{x}) \mathrm{e}^{-\mathrm{i}\boldsymbol{k}\cdot\boldsymbol{x}} d\boldsymbol{x} \tag{10}$$

Since $\boldsymbol{u}^*(\boldsymbol{k}) = \boldsymbol{u}(-\boldsymbol{k})$ (9) can also be written as

$$\left\langle u_i(\boldsymbol{k}) u_j(\boldsymbol{k'}) \right\rangle = \Phi_{ij}(\boldsymbol{k}) \delta(\boldsymbol{k} + \boldsymbol{k'}) \tag{11}$$

2.1.1. Rotor averaged wind speed Substituting (8) into the rotor averaged wind speed (5) and changing the order of integration gives

$$\begin{aligned} u_R(x_1,0,0) &= \frac{1}{\pi R^2}\int u_1(\boldsymbol{k})\mathrm{e}^{\mathrm{i}k_1x_1}\iint\limits_{\text{rotor}}\mathrm{e}^{\mathrm{i}(k_2x_2+k_3x_3)}dx_2dx_3d\boldsymbol{k} \\ &= \int u_1(\boldsymbol{k})\mathrm{e}^{\mathrm{i}k_1x_1}\frac{2J_1(\kappa R)}{\kappa R}d\boldsymbol{k}, \end{aligned} \tag{12}$$

where $\kappa=\sqrt{k_2^2+k_3^2}$ and J is the Bessel function of the first kind. We have also assumed that the rotor center is on the x_1-axis ($x_2=x_3=0$).

2.1.2. Lidar velocity Substituting (8) into the line-of-sight velocity measured by a single beam (2) and reversing the order of integration gives

$$\begin{aligned} v_i &= \int \boldsymbol{n}_i\cdot\boldsymbol{u}(\boldsymbol{k})\mathrm{e}^{\mathrm{i}k_1x_1}\int_{-\infty}^{\infty}\mathrm{e}^{\mathrm{i}s\boldsymbol{k}\cdot\boldsymbol{n}_i}\phi(s-d_f)dsd\boldsymbol{k} \\ &= \int \boldsymbol{n}_i\cdot\boldsymbol{u}(\boldsymbol{k})\mathrm{e}^{\mathrm{i}k_1x_1}\mathrm{e}^{\mathrm{i}d_f\boldsymbol{k}\cdot\boldsymbol{n}_i}\exp\left(-z_R\left|\boldsymbol{k}\cdot\boldsymbol{n}_i\right|\right)d\boldsymbol{k}. \end{aligned} \tag{13}$$

Again we assume that the lidar instrument is on the x_1-axis.

2.1.3. Squared error variance Expanding the right hand side of (7) gives three terms. The simplest is

$$\begin{aligned} &\left\langle u_R^2(\boldsymbol{x}-\Delta x\boldsymbol{e}_1)\right\rangle \\ &= \left\langle\int u_1(\boldsymbol{k})\mathrm{e}^{\mathrm{i}k_1(x-\Delta x)}\frac{2J_1(\kappa R)}{\kappa R}d\boldsymbol{k}\int u_1(\boldsymbol{k}')\mathrm{e}^{\mathrm{i}k_1'(x-\Delta x)}\frac{2J_1(\kappa' R)}{\kappa' R}d\boldsymbol{k}'\right\rangle \\ &= \iint\delta(\boldsymbol{k}+\boldsymbol{k}')\phi_{11}(\boldsymbol{k})\mathrm{e}^{\mathrm{i}k_1(x-\Delta x)}\frac{2J_1(\kappa R)}{\kappa R}\mathrm{e}^{\mathrm{i}k_1'(x-\Delta x)}\frac{2J_1(\kappa' R)}{\kappa' R}d\boldsymbol{k}'d\boldsymbol{k} \\ &= \int\frac{4J_1^2(\kappa R)}{\kappa^2R^2}\Phi_{11}(\boldsymbol{k})d\boldsymbol{k} \end{aligned} \tag{14}$$

using the definition of the spectral tensor (11). The other squared term in (7) is

$$\left\langle u_L^2(\boldsymbol{x})\right\rangle = \langle m_iv_im_jv_j\rangle = m_i\left\langle v_iv_j\right\rangle m_j \tag{15}$$

so we need to calculate the covariances between the lidar beam velocities. These are

$$\langle v_iv_j\rangle = \int n_{ik}\Phi_{kl}n_{jl}\exp\left[\mathrm{i}d_f\boldsymbol{k}\cdot(\boldsymbol{n}_i-\boldsymbol{n}_j)-z_R\left(\left|\boldsymbol{k}\cdot\boldsymbol{n}_i\right|+\left|\boldsymbol{k}\cdot\boldsymbol{n}_j\right|\right)\right]d\boldsymbol{k} \tag{16}$$

Finally, the cross-term

$$\langle u_L(\boldsymbol{x})u_R(\boldsymbol{x}-\Delta x\boldsymbol{e}_1)\rangle = m_i\left\langle v_i(\boldsymbol{x})u_R(\boldsymbol{x}-\Delta x\boldsymbol{e}_1)\right\rangle \tag{17}$$

calls for an evaluation of the covariance between the ith lidar beam velocity and the rotor average

$$\begin{aligned} &\langle v_i(\boldsymbol{x})u_R(\boldsymbol{x}-\Delta x\boldsymbol{e}_1)\rangle \\ &= \int n_{ij}\Phi_{j1}(\boldsymbol{k})\mathrm{e}^{\mathrm{i}\left[d_f\boldsymbol{k}\cdot\boldsymbol{n}_i+k_1\Delta x\right]}\frac{2J_1(\kappa R)}{\kappa R}\exp\left(-z_R\left|\boldsymbol{k}\cdot\boldsymbol{n}_i\right|\right)d\boldsymbol{k}, \end{aligned} \tag{18}$$

where (12) and (13) are combined with (11). Now the error variance (7) can be calculated from (14), (16) and (18) by expanding (7) as

$$\sigma_e^2 = \left\langle u_R^2\right\rangle + m_i\left\langle v_iv_j\right\rangle m_j - 2m_i\left\langle v_i(\boldsymbol{x})u_R(\boldsymbol{x}-\Delta x\boldsymbol{e}_1)\right\rangle. \tag{19}$$

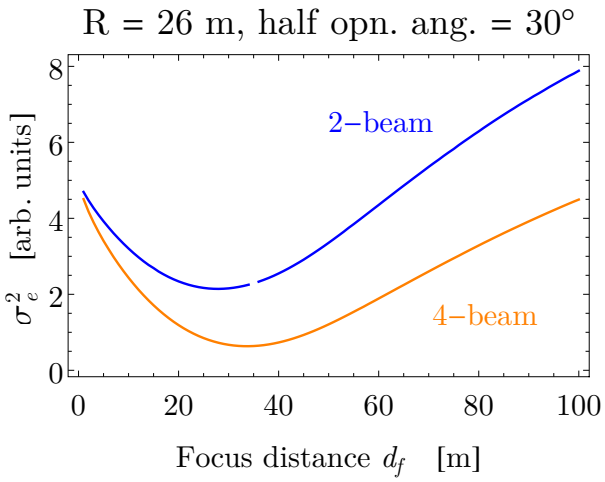

Figure 2. The mean squared difference of the rotor averaged wind speed and the lidar derived as a function of focus distance for the four-beam configuration shown in figure 1 and a two beam configuration with horizontal beams. The diameter of the rotor is 52 m and the half opening angle is 30°.

2.2. A few results from the theory

The squared difference between the rotor averaged wind speed and the one derived from the lidar can now be easily calculated as an integral over the spectral tensor and many beam configurations can be investigated rapidly. An example is shown in figure 2. It can be seen that the four beam configuration has a significantly smaller difference than the two-beam configuration. The minima obtained around a focus distance of 30 m are a consequence of the opposing effects of the focus volume increasing quadratically with d_f and an improved alignment of the beams with the mean wind direction with increasing d_f. We can also show that adding more beams to the system has diminishing value beyond four to six beams. The model can also be used to position the beam optimally within the rotor area.

It should be emphasized that the model use Taylor's hypothesis and thus does not take into account the mutation of turbulence as it travels from the lidar measurement volumes to the rotor. This effect will in general put the optimal focus distance closer to the rotor than predicted by the theory.

3. Numerical simulations

In this section numerical simulations are used to find the optimum configuration of the lidar. Mann turbulence model [7] is used to produce the turbulence box. The parameters of the turbulence box are chosen to be $\alpha\varepsilon^{2/3} = 1$, $L = 42\ m$ and $\Gamma = 3.9$.

A lidar model is developed based on the physics of the lidar device. The weighting function is given in (3) in which z_R (the Rayleigh length) is defined as:

$$z_R = \frac{\lambda}{\pi}\frac{r^2}{\alpha_0^2} \tag{20}$$

where λ is the wavelength of the emitted radiation, r is the focus distance and α_0 is the effective radius of telescope used for emitting and receiving the laser signal. The numerical values for the parameters are chosen to be: $\lambda = 1.565\ \mu m$ and $\alpha_0 = 0.02\ m$.

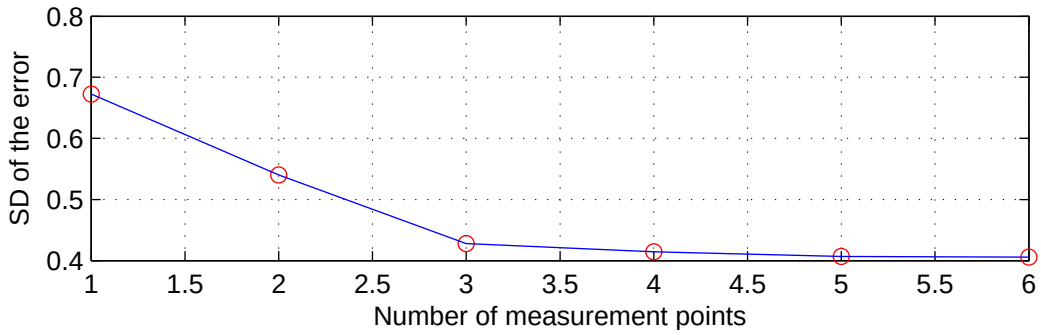

Figure 3. Minimum achievable standard deviation as function of number of measurement points

For the comparison purpose, it is assumed that perfect measurement of the wind speed on the rotor for all the grid points is available. This means the effect of the wind speed on the rotor can be calculated by proper weighting of the point wind speeds:

$$v_e = \int_0^{2\pi} \int_0^R v(r,\theta) r dr d\theta / \int_0^{2\pi} \int_0^R r dr d\theta \tag{21}$$

in which $R = 63m$ is the rotor radius. Time series of the wind speed from the lidar model (v_L) is compared against the effective wind speed (v_e) calculated from equation 21. The error between the two time series is calculated neglecting the advection time as $e = v_L - v_e$. The measurements for the rotor effective wind speed and the lidar are done on the same plane in the turbulence box and the plane is moved along the turbulence box. It can be shown that the error has a Gaussian distribution. The standard deviation of the error is used as a measure of performance of the lidar.

4. Results

In this section the results of the two methods explained in sections 2 and 3 are presented and compared. Figure 3 shows the minimum achievable standard deviation for different number of measurement points. The results show that the best achievable performance drops significantly between the first 3 points and after the 4th point the performance does not increase very much. Based on this result and also the extra cost of adding more measurement points, it was decided to use a lidar with 4 measurement points.

Figures 4 and 5 show the contour curves of the standard deviation of the error as a function of the location of the measurement point in the $x - y$ plane. The results are for the lidar with 4 measurement points. x is along the horizontal line, upstream the wind turbine and apposite to the wind direction. y is the lateral distance of the measurement point from the center of the rotor. Figure 5 shows the results based on the theoretical method explained in section 2 and figure 4 shows the results obtained using numerical simulations. The results are slightly different. One reason for the difference can be that the simulation is done only for one turbulence box while it needs to be done for several turbulence boxes with different seed numbers in order to have better statistics. From the obtained results it is possible to find the best configuration for the 4-beam lidar. For the theoretical analysis, the best configuration is to focus the lidar at $2.75R$ upstream and $0.55R$ off the center of the rotor. The simulation results show that the best configuration is to focus the lidar at $3.25R$ upstream and $0.6R$ off the center of the rotor. From these results the half opening angle θ and the LOS measurement distances L_{los} can be calculated. For the theoretical case they are: $\theta = 11.3$ degrees and $L_{los} = 2.8R$ and for the simulation case they are: $\theta = 10.4$ degrees and $L_{los} = 3.30R$.

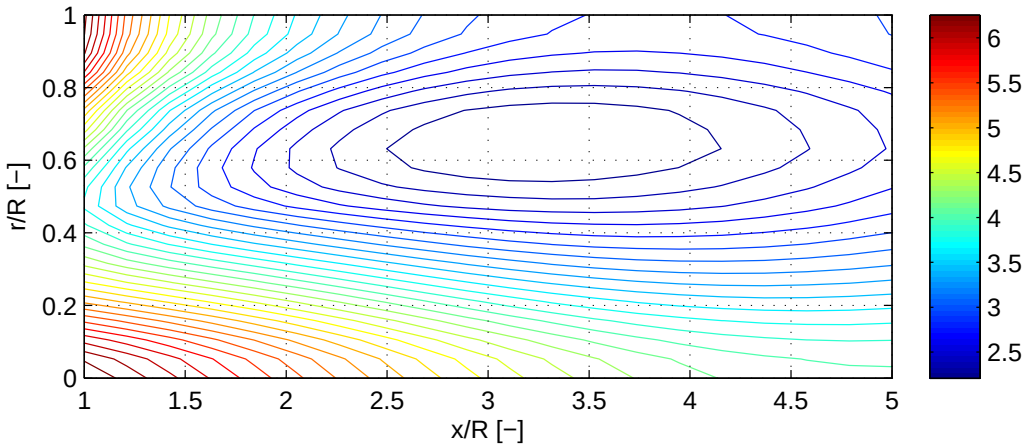

Figure 4. Simulation results for the standard deviation of the measurement error (R stands for rotor radius)

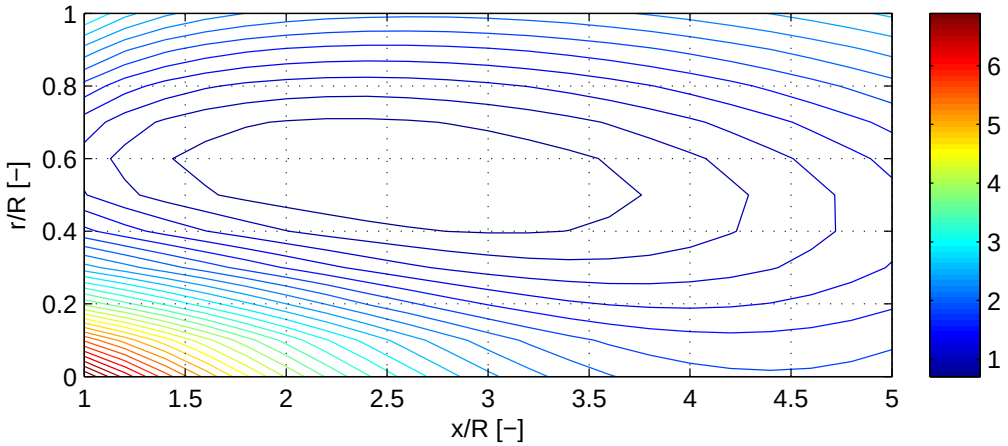

Figure 5. Theoretical results for the standard deviation of the measurement error (R stands for rotor radius)

5. Conclusion

The paper presents two approaches for analyzing and optimally selecting best configurations for a lidar with limited number of measurement points. First it was shown how the measurement accuracy changes with different number of measurement points and argued that a good trade-off between the cost of adding more measurement points and accuracy of measurements can be achieved for a lidar with 4 measurement points. Later it was shown through both theoretical and simulation analysis how to configure the focus distance and half opening angle of the lidar.

References

[1] N. Angelou, J. Mann, M. Sjöholm, and M. Courtney. Direct measurement of the spectral transfer function of a laser based anemometer. *Rev. Sci. Instrum.*, 83:033111, 2012.
[2] G. K. Batchelor. *The theory of homogeneous turbulence.* Cambridge University, 1953.
[3] A. Davenport. The prediction of the response of structures to gusty wind. *Safety of structures under dynamic loading*, 1:257–284, 1977.
[4] N. K. Dimitrov and B. S. Lazarov. Reducing wind turbine load simulation uncertainties by means of a

constrained gaussian turbulence field. *Proceedings of the 12th International Conference on Applications of Statistics and Probability in Civil Engineering (icasp12)*, pages –, 2015.

[5] P. A. Fleming, A. K. Scholbrock, A. Jehu, S. Davoust, E. Osler, A. D. Wright, and A. Clifton. Field-test results using a nacelle-mounted lidar for improving wind turbine power capture by reducing yaw misalignment. *Journal of Physics. Conference Series*, 524(1):–, 2014.

[6] J. Laks, L. Y. Pao, E. Simley, A. Wright, N. Kelley, and B. Jonkman. Model predictive control using preview measurements from lidar. *Proc. AIAA Aerospace Sciences Meeting, Orlando, FL*, pages –, 2011.

[7] J. Mann. The spatial structure of neutral atmospheric surface-layer turbulence. *Journal of Fluid Mechanics*, 273:141–68, 1994.

[8] J. Mann. The spatial structure of neutral atmospheric surface-layer turbulence. *J. Fluid Mech.*, 273:141–168, 1994.

[9] M. Mirzaei, N. K. Poulsen, and H. H. Niemann. Individual pitch control using lidar measurements. In *IEEE Multiconference on Systems and Control*, Dubrovnik, Croatia, 2012.

[10] T. Mizuno and H. A. Panofsky. The validity of Taylor's hypothesis in the atmospheric surface layer. *Boundary-Layer Meteorol.*, 9:375–380, 1975.

[11] P. J. Rodrigo and C. Pedersen. Field performance of an all-semiconductor laser coherent Doppler lidar. *Optics Letters*, 37(12):2277–2279, June 2012.

[12] D. Schlipf, P. W. Cheng, and J. Mann. Model of the correlation between lidar systems and wind turbines for lidar-assisted control. *Journal of Atmospheric and Oceanic Technology*, 30:2233, 2013.

[13] D. Schlipf and M. Kühn. Prospects of a collective pitch control by means of predictive disturbance compensation assisted by wind speed measurements. In *Proceedings of the German Wind Energy Conference, DEWEK*, 2008.

[14] C. M. Sonnenschein and F. A. Horrigan. Signal-to-noise relationships for coaxial systems that heterodyne backscatter from the atmosphere. *Applied Optics*, 10(7):1600, 1971.